CrossMark

Full-scale linear cutting test in Chongqing Sandstone and the comparison with field TBM excavation performance

Yucong Pan[1,3,4] · Quansheng Liu[1] · Xiaoxuan Kong[1] · Jianping Liu[2,3,4] · Xingxin Peng[3,4] · Qi Liu[1]

Abstract

In this study, determination of some machine parameters and performance prediction for tunnel boring machine (TBM) are conducted based on laboratory rock cutting test. Firstly, laboratory full-scale linear cutting test is carried out using 432-mm CCS (constant cross section) disc cutter in Chongqing Sandstone. Then, the input parameters for TBM cutterhead design are extracted; some TBM specifications are determined and then compared to the manufactured values. Finally, laboratory full-scale linear cutting test results are compared with the field TBM excavation performance data collected in Chongqing Yangtze River Tunnel. Results show that laboratory full-scale linear cutting test results, combined with some engineering considerations, can be used for the preliminary and rough design of TBM machine capacity. Meanwhile, combined with some modification factors, it can also well predict the field TBM excavation performance.

Keywords Cutterhead design · Disc cutter · Excavation performance · Linear cutting machine (LCM) · Mechanical rock breakage · Tunnel boring machine (TBM)

1 Introduction

Accurate and reliable performance prediction for mechanical excavation projects is very important for their successful and economic completion. That is because the machine specifications and time/logistical schedules are usually determined based on the predicted machine requirement and excavation rate/production. Therefore,

✉ Quansheng Liu
liuqs@whrsm.ac.cn

1   Key Laboratory of Safety for Geotechnical and Structural Engineering of Hubei Province, School of Civil Engineering, Wuhan University, Wuhan 430072, Hubei, People's Republic of China

2   College of Water Conservancy and Hydropower Engineering, Sichuan Agricultural University, Ya'an 625014, Sichuan, People's Republic of China

3   State Key Laboratory of Geomechanics and Geotechnical Engineering, Institute of Rock and Soil Mechanics, Chinese Academy of Sciences, Wuhan 430071, Hubei, People's Republic of China

4   University of Chinese Academy of Sciences, Beijing 100049, People's Republic of China

one important issue when using tunnel boring machines (TBMs) is how to model the machine performance in different excavation scenarios. These excavation scenarios include, for example, tunneling under high groundwater pressure, high ground temperature or high in situ stress, excavating in hard massive rock mass, weak fractured rock mass or mixed ground condition. This hot topic concerning on rock cutting force and efficiency under TBM cutter/cutterhead has been widely investigated by using theoretical, empirical, numerical, experimental methods, laboratory prototype machine testing or field TBM penetration test [4, 6, 8, 9, 17, 20, 37, 40, 43, 49]. Recently, Gong et al. [29], Liu et al. [30] and Ramezanzadeh et al. [38] have made detailed and excellent literature reviews on the adverse geological conditions and performance prediction models for TBM tunneling. Moreover, for the advantages over the simplistic small-scale tests and expensive in situ tests, laboratory full-scale linear cutting tests have been proved to be the most reliable and accurate approach to reveal the rock cutting mechanism by TBM cutter, to design TBM cutterhead and then predict its excavation performance [2, 9–11, 13, 18, 19, 25–28, 39, 42, 46, 50].

To capture the rock cutting process and characteristics by TBM cutting tools, rock cutting forces and rock cutting products have been deeply analyzed using linear cutting machine (LCM) tests. Cho et al. [10] presented the results of LCM tests carried out under various cutting conditions to assess the cutting performance and cutting efficiency of TBM disc cutter in Korean granitic rock using photogrammetric measurement. Gertsch et al. [20] provided some insights into the performance prediction for a TBM operating in hard and brittle crystalline rock of moderate strength with the LCM test results obtained in Colorado Red Granite. Balci and Tumac [3] and Tumac and Balci [46] conducted LCM tests in three kinds of low-strength rocks to investigate the effects of different rock structural properties and disc cutter types (V- or CCS-type) on rock cuttability and rock cutting characteristics (Here, "CCS" refers to "constant cross section"). Abu Bakar et al. [1] analyzed the results of grain size distribution and its relationship with specific energy and cutting geometry by evaluating the fragments from disc cutting dry and saturated sandstone. Tuncdemir et al. [47] carried out LCM tests using chisel picks, conical cutters, V and CCS real-life disc cutters to explain the basic rules governing the relationships between specific energy and chip sizes. Ma et al. [35, 36] studied the effects of different confining stressed conditions on the force–time curve, rock cutting force, rock boreability index, chipping thickness and specific energy. Yin et al. [50] investigated the influences of joint spacing on the rock fragmentation process by TBM disc cutter through analyzing the rock cutting force, crack initiation/propagation and rock chips. These researches have provided many inspiring and penetrating insights on the mechanical rock breakage mechanism for different rock types, different cutting tools, different confining stressed conditions and different rock intactness degrees.

TBM cutterhead design and performance prediction using laboratory full-scale linear cutting tests and comparison between the predicted and field TBM excavation performances have also been extensively and successfully conducted. Balci [2] investigated the correlation of full-scale linear rock cutting tests in intact rock samples with field performance of a TBM in highly fractured rock formation. Balci and Tumac [3] compared the experimental, theoretical and field rock cutting results related to rock cuttability by taking into account the rock properties and V-type disc cutter's forces. Bilgin et al. [5] carried out the determination of some design parameters and performance prediction of TBM using full-scale rock cutting test in the main rock formations encountered in Kadikoy-Kartal Metro Tunnels. Copur et al. [13] predicted the performance of earth pressure balance (EPB) TBMs by using a stochastic model implemented into a deterministic model and then verified it by measuring the field performance of

two EPB TBMs excavating component rocks in semi-closed mode. These researches showed that fractured characteristics and geological discontinuities of the rock formation can tremendously affect the TBM performance, and the predicted values using full-scale linear cutting tests may differ from the field data to some extent, and only in component rock formations the laboratory results can be in good agreement with the field results [2, 5]. Also, Fukui and Okubo [15] suggested a method for calculating rock strength and rock mass classification at the tunnel face from the cutting force exerted by the TBM based on the results of laboratory experiments. Then, they applied this method for a tunnel through granite and a tunnel through mixed strata containing multiple rock types, which proved quite successful in Japanese tunnel excavations [16]. Cardu et al. [7] developed an intermediate linear cutting machine (ILCM) and compared the experimental results with the CSM (Colorado School of Mines) model and the NTNU (Norwegian University of Science and Technology) model. Then, they made the preliminary TBM cutterhead design by using the NTNU model and compared the designed results with the field TBM excavation results.

This study conducted the laboratory full-scale linear cutting test in Chongqing Sandstone and analyzed the field TBM excavation performance in Chongqing Yangtze River Tunnel. Mainly, three aspects concerning on rock cutting and tunnel excavation sciences are investigated. Firstly, the changing trends of disc cutter cutting force, cutting coefficient, force acting point, rock boreability index and rock cutting specific energy with increasing cutter penetration depth are deeply analyzed. Then, the input parameters for TBM cutterhead design are extracted; some TBM specifications are determined and then compared to the manufactured values. Finally, the laboratory rock cutting test results are compared with the field TBM excavation performance data to show the similarities and differences between them. Results show that laboratory full-scale linear cutting test results, combined with some engineering considerations, can be used for the preliminary and rough design of TBM machine capacity. Meanwhile, combined with some modification factors, it can also well predict the field TBM excavation performance.

2 Laboratory full-scale linear cutting test in Chongqing Sandstone

2.1 Test description

2.1.1 Chongqing Sandstone

The rock samples used for laboratory full-scale linear cutting test are obtained in the rock formation where TBM

tunnels through. After that, some rock samples are cut into large cubic blocks with the dimension $1.0 \times 1.0 \times 0.6$ m while some of them are trimmed into standard cylinder samples with the diameter 50.0 mm and length 100.0 or 50.0 mm. All the strength and deformation parameters are obtained based on the ISRM-suggested testing procedures [48]. Table 1 shows some important physical and mechanical properties of the Chongqing Sandstone. As seen, it is one kind of hard brittle sedimentary rock with uniaxial compressive strength about 60.76 MPa and brittleness index about 33.6. According to Song [45], Chongqing Sandstone is mainly composed of feldspar, quartz and small quantity of mica and calcite, accounting for about 67, 30 and 3%, respectively. Permeability of the Chongqing Sandstone mainly varies from 0.10 to 0.30 md, but its maximum value can be up to 3.65 md. It indicates that this rock formation is generally impermeable, but it may have high potential to being penetrated by groundwater flow at some weak/fractured areas.

2.1.2 Full-scale linear cutting machine

Figure 1a shows the mechanical rock breakage experimental platform developed at Beijing University of Technology. Gong et al. [27] introduced the design conception and constitution of this linear cutting machine in detail and then validated its function using normal linear cutting tests, confining stressed linear cutting tests and rotary cutting tests. According to Gong et al. [25–28], Ma et al. [35, 36] and Yin et al. [50], this testing machine can successfully consider the influence of rock mass structure (e.g., joint spacing), high in situ stress, cutterhead rotation and rock cutting by multi-number and multi-type cutters on the mechanical rock breakage process. This study mainly employs its non-stressed linear cutting function by using one CCS disc cutter with diameter 432 mm and tip width 15 mm (Table 2).

Table 1 Some physical and mechanical properties of Chongqing Sandstone

Physical and mechanical properties	Chongqing Sandstone
Uniaxial compressive strength, σ_c (MPa)	60.76
Brazilian tensile strength, σ_t (MPa)	1.81
Static elasticity modulus, E (GPa)	13.63
Poisson's ratio, v	0.232
Density, ρ (g/cm^3)	2.308
P wave velocity, v_P (m/s)	2500–2700
Permeability, k (md)	0.10–0.30, up to 3.65

2.1.3 Test procedure and data analysis

Figures 1b and c shows the rock breakage surface and rock breakage phenomenon for the laboratory full-scale linear cutting test in Chongqing Sandstone. Prior to the formal test, top surface of the rock block is fully preconditioned to create a damaged rock surface similar to the real tunnel face. During the test, cutter spacing is set to 80 mm, so nine cutting lines (i.e., seven interactive cuts and two exterior cuts) are created for one cutting pass at first (Fig. 1b), but only three of them (i.e., the fourth, fifth and sixth cuts) are remained at last when using cutter penetration depth 9 mm for the fourth cutting pass. During the test, cutter penetration depth increases from 1 to 9 mm with the increment 1 or 2 mm for each time; therefore, the selected cutter penetration depths are 1, 2, 3, 4, 5, 7 and 9 mm (Table 2). The increment is added to the cutter penetration depth after four or five cutting passes are finished using one cutter penetration depth; then, the following cutting passes using larger cutter penetration depth are started. For each cutting line, the three-directional forces acting on the disc cutter (i.e., normal force, rolling force and side force) are recorded and displayed real-timely (Fig. 1c, d). These rock cutting forces are then averaged to obtain the laboratory disc cutter normal force and rolling force (i.e., FN_{lab} and FR_{lab}). Note here that the non-representative part of the rock cutting forces should be excluded first, i.e., the data obtained from the first or two cutting passes after enlarging cutter penetration depth, obtained at the start and end of each cutting line and obtained from the two exterior cutting lines. After each cutting pass, rock breakage surface is carefully cleaned and rock mucks are well collected (Fig. 1b, c). These rock cutting products are then subjected to sieving analysis using 11 sets of mesh sizes (Fig. 1e). The rock mucks remaining at each sieve after the sieving procedure are weighted to calculate the yield V_c and the laboratory rock cutting specific energy SE_{lab}. The former one is the rock cutting volume per cutting distance for each cutting line, and the latter one is the cutting energy required to cut a unit volume of rock, obtained by dividing the mean disc cutter rolling force FR_{lab} using the yield V_c. Table 3 shows the laboratory full-scale linear cutting test results for Chongqing Sandstone. Laboratory disc cutter cutting coefficient CC_{lab} is calculated by dividing the mean disc cutter rolling force FR_{lab} using the mean disc cutter normal force FN_{lab}. Laboratory normalized resultant force of the disc cutter NRF_{lab} is calculated by dividing the resultant angle of the disc cutter using the rock-cutter contact angle for each cutter penetration depth (angles are all referenced to the vertical direction). Detailed information about this parameter can be found in Table 3 and Gertsch et al. [20]. Laboratory rock boreability index BI_{lab} is calculated by
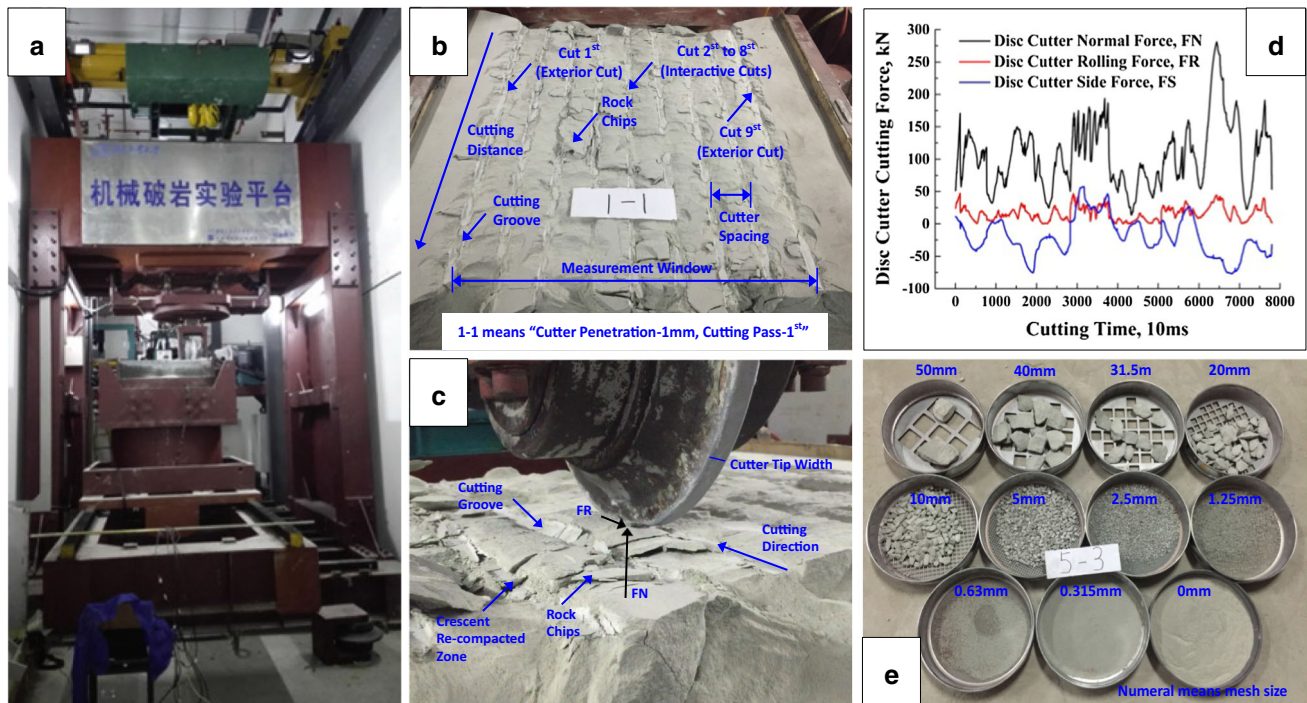
Fig. 1 Laboratory full-scale linear cutting test in Chongqing Sandstone. **a** Mechanical rock breakage experimental platform, **b** rock breakage surface, **c** rock breakage phenomena, **d** rock cutting forces and **e** rock muck analysis

Table 2 Some experimental parameters for the laboratory full-scale linear cutting test in Chongqing Sandstone

Experimental parameters	Chongqing Sandstone
Disc cutter diameter, D (mm)	432
Disc cutter tip width, T (mm)	15
Cutter spacing, s (mm)	80
Penetration depth, p (mm)	1, 2, 3, 4, 5, 7, 9
Cutting velocity, v_0 (mm/s)	20

dividing the mean disc cutter normal force FN_{lab} using the cutter penetration depth p. The schematic diagram of the cutting parameters is shown in Fig. 2, and the changing trends of the rock cutting results with increasing cutter penetration depth will be investigated detailedly in Sect. 2.2.

2.2 Result analysis

2.2.1 Disc cutter normal and rolling forces

Disc cutter normal force FN determines whether the disc cutter can efficiently penetrate into the rock surface and then crack it or not. It is also the main driving factor for crack initiation/propagation and rock chipping/spalling. Thus, normal force-indentation models have been widely

studied by using theoretical, numerical and experimental methodologies [21, 22, 31–34, 43, 44]. Unlike the over-simplified modeling of the vertical indentation process, Fig. 3 shows the more realistic FN $\sim p$ curve obtained from laboratory full-scale linear cutting test. As seen, cutter penetration depth increases when disc cutter normal force increases, and the increasing trend becomes more rapid at higher disc cutter normal force. Or in other words, disc cutter normal force increases when cutter penetration depth increases, but the increasing trend becomes less rapid at higher cutter penetration depth. Therefore, one critical threshold can be marked at cutter penetration depth 3.0 mm and disc cutter normal force 76.56 kN. Below this critical threshold, for cutter penetration depth increasing from 1 to 2 mm or from 2 to 3 mm, large increment about 16 kN is required for disc cutter normal force. Above this critical threshold, for cutter penetration depth increasing by 1 mm, only small increment about 5 kN is required for disc cutter normal force. That is to say, only when above this critical threshold can effective rock penetration and cutting be fulfilled. Thus, this critical cutter penetration depth indicates the start of efficient rock cutting by TBM disc cutter. This critical threshold phenomenon for mechanical rock breakage from difficulty to ease has also been noted by Gertsch et al. [20] and Gong et al. [25] in laboratory full-scale linear cutting tests and by Gong et al. [23] and Yin et al. [49] in field TBM penetration tests.

Table 3 Results of the laboratory full-scale linear cutting test in Chongqing Sandstone

p (mm)	FN_{lab} (kN)	FR_{lab} (kN)	CC_{lab} (%)	NRF_{lab}^{a} (ratio)	BI_{lab} (kN/mm)	SE_{lab} (MJ/m³)
1	43.95	2.89	6.58	0.6821	44.00	95.3
2	60.85	4.28	7.03	0.5156	30.45	39.6
3	76.56	6.30	8.23	0.4920	25.53	30.1
4	82.58	7.71	9.34	0.4830	20.65	23.4
5	87.38	9.81	11.23	0.5186	17.48	18.7
7	97.09	12.29	12.66	0.4932	13.87	18.9
9	103.43	17.66	17.07	0.5838	11.49	29.8

p cutter penetration depth, FN_{lab} laboratory disc cutter normal force, FR_{lab} laboratory disc cutter rolling force, CC_{lab} laboratory disc cutter cutting coefficient, NRF_{lab} laboratory disc cutter normalized resultant force, BI_{lab} laboratory rock boreability index, SE_{lab} laboratory rock cutting specific energy

[a] NRF_{lab} is calculated by dividing the resultant angle of the disc cutter cutting force β using the rock-cutter contact angle φ for each cutter penetration depth. The resultant angle of the disc cutter cutting force β is calculated as: $\beta = \arctan(FR_{lab}/FN_{lab})$, and the rock-cutter contact angle φ for each cutter penetration depth is calculated as: $\varphi = \arccos((0.5D - p)/0.5D)$. Thus, NRF_{lab} is calculated as

$$NRF_{lab} = \frac{\beta}{\varphi} = \frac{\arctan(FR_{lab}/FN_{lab})}{\arccos((0.5D-p)/0.5D)}$$

As induced by the continuous rolling movement of the disc cutter, disc cutter rolling force FR can only be taken into consideration in linear or rotary cutting tests, not any indentation-type studies. This parameter is of great importance because it is used to determine the required machine torque and power. On the one hand, disc cutter rolling force should be large enough to offer the rotation moment that can overcome the starting torque to avoid disc cutter flat wear; on the other hand, it should also be not too
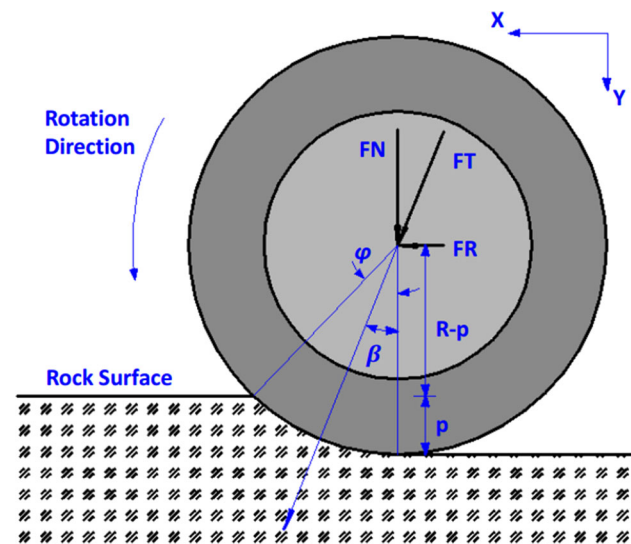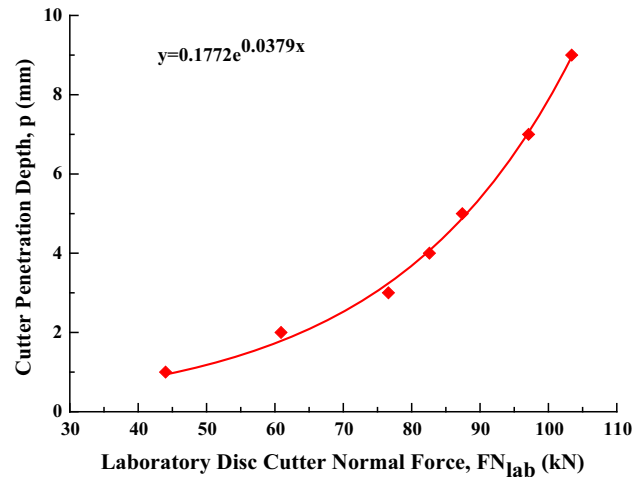

Fig. 3 Relation between laboratory disc cutter normal force (FN_{lab}) and cutter penetration depth (p)

large that may damage the cutter bearing and exceed the machine capability. As seen in Fig. 4, disc cutter rolling force increases continuously and steadily in almost linear function form when cutter penetration depth increases. This changing trend generally coincides with the famous CCS disc cutter cutting force estimation approach [40, 41], where FR is expressed with p using power of 5/6: FR $\sim$ $p^{5/6}$. Unlike disc cutter normal force, no critical threshold can be marked for disc cutter rolling force at any cutter penetration depth. Therefore, cutter bearing and saddle should have the capability to bear the continuously and rapidly increasing transversal force and bending moment when cutter penetration depth increases. As seen in Fig. 4, when disc cutter penetrates 1 mm deeper, increment about 1.8 kN is required for disc cutter rolling force. Though this value seems lower than the increment for disc cutter
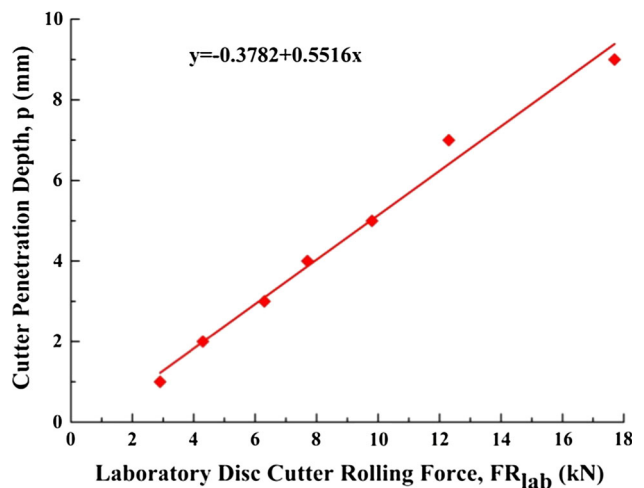

Fig. 2 Schematic diagram for normal and rolling forces acting on the disc cutter

Fig. 4 Relation between laboratory disc cutter rolling force (FR_{lab}) and cutter penetration depth (p)

normal force (5 or 16 kN), it matters quite significantly because disc cutter rolling force is also much lower than disc cutter normal force.

2.2.2 Disc cutter cutting coefficient and normalized resultant force

Disc cutter cutting coefficient CC and normalized resultant force NRF can represent the relative relations between the vertical and horizontal components of the disc cutter resultant force. The former one indicates the proportion of disc cutter normal force and rolling force in disc cutter resultant force, and it also indicates the amount of cutter-head torque required for a given amount of cutterhead thrust: The higher the CC, the higher the cutterhead torque needed by the TBM [20]. As seen in Fig. 5, disc cutter cutting coefficient increases almost linearly when cutter penetration depth increases. That is to say, the proportion of disc cutter rolling force in disc cutter resultant force keeps increasing rapidly when disc cutter penetrates deeper, and meanwhile cutterhead torque increases quickly with faster speed than cutterhead thrust. Like disc cutter rolling force, no critical threshold can be marked for disc cutter cutting coefficient at any cutter penetration depth. As seen in Fig. 5, increment about 1.2% is added to disc cutter cutting coefficient as disc cutter penetrates every millimeter deeper.

Disc cutter normalized resultant force NRF denotes the acting point and acting direction of the disc cutter resultant force and is usually assumed to be 0.5000 [40, 43]. This assumption means that disc cutter resultant force acts on the middle point of the rock-cutter contact arc and bisects the rock-cutter contact angle to pass through the cutter hub [20]. When it is smaller than 0.5000, disc cutter resultant force acts below the midpoint and stronger indentation

effect occurs during rock disc cutting; when it is larger than 0.5000, disc cutter resultant force acts above the midpoint and higher transversal force acts on the disc cutter during rock disc cutting. As seen in Fig. 6, most of these NRF$_{lab}$ values are locate above the 0.5000 line, averaging at about 0.5389. It indicates that disc cutter resultant force generally acts slightly higher than the assumed midpoint and also larger transversal force (impact) is exposed to the disc cutter when cutting Chongqing Sandstone. Two much higher NRF$_{lab}$ values (about 0.6821 and 0.5838) can be marked at low cutter penetration depth (i.e., 1 mm) and large cutter penetration depth (i.e., 9 mm), and smaller NRF$_{lab}$ values (about 0.5000) can be marked at the medium cutter penetration depth range (i.e., from 1 to 9 mm).

2.2.3 Rock boreability index and rock cutting specific energy

Rock boreability index BI describes the ease or difficulty with which a rock type can be penetrated by a TBM [12, 23]. It is defined as the disc cutter normal force required for penetrating into the rock surface at every millimeter. As seen in Fig. 7, there exists power function relation between rock boreability index and cutter penetration depth, in good agreement with the previous laboratory linear cutting tests [2, 36] and field TBM excavation performance [2, 23, 49]. Moreover, critical threshold of cutter penetration depth 5.0 mm can be marked for rock boreability index. Below it, rock boreability index is high and decreases rapidly; above it, rock boreability index is low and decreases slowly. Specific rock mass boreability index (SRMBI), defined by Gong et al. [24] as the rock boreability index at the penetration rate equal to 1.0 mm per revolution, is calculated as 44.66 kN/mm for
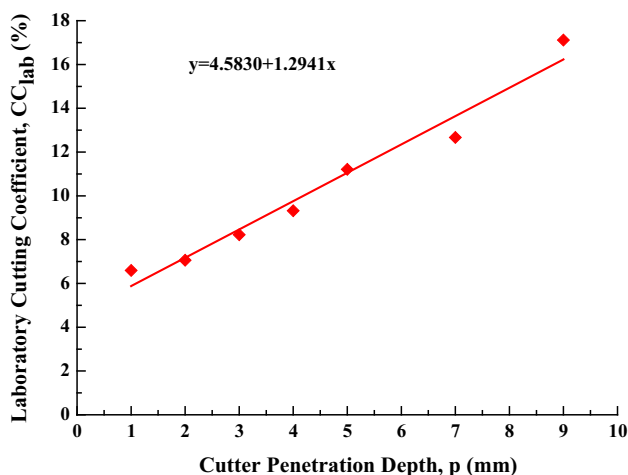

Fig. 5 Relation between laboratory cutting coefficient (CC$_{lab}$) and cutter penetration depth (p)
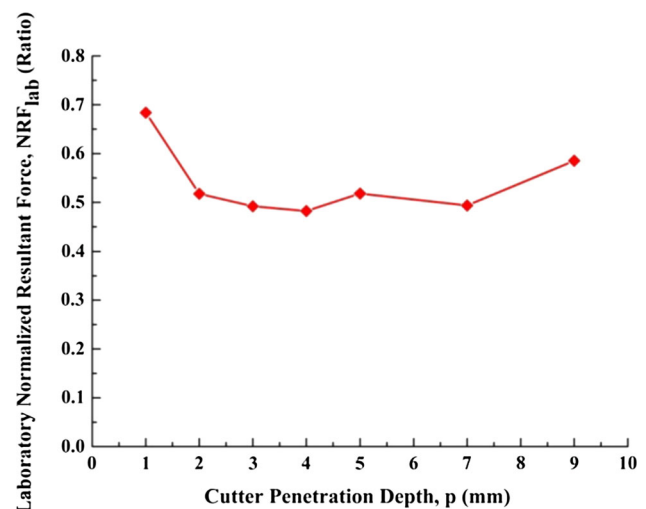

Fig. 6 Relation between laboratory normalized resultant force (NRF$_{lab}$) and cutter penetration depth (p)
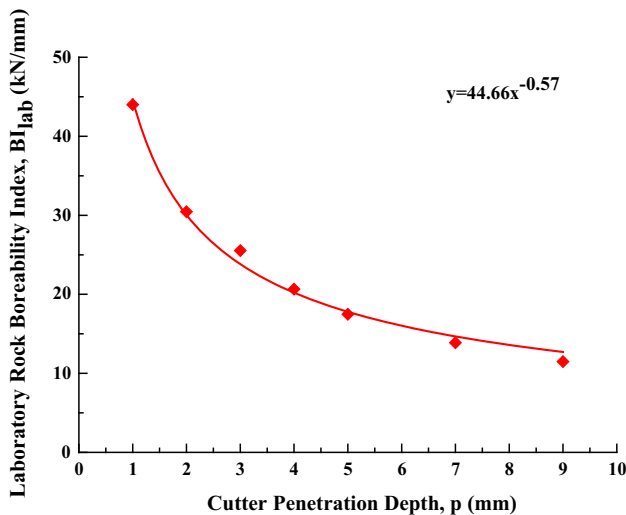
Fig. 7 Relation between laboratory rock boreability index (BI_{lab}) and cutter penetration depth (p)

Fig. 8 Relation between laboratory rock cutting specific energy (SE_{lab}) and cutter penetration depth (p)

Chongqing Sandstone with uniaxial compressive strength 60.76 MPa. The power exponent of -0.75 is suggested to relate the specific rock mass boreability index to the rock boreability index at any cutter penetration depth [23, 49]. However, larger power exponents can be found in laboratory full-scale linear cutting tests conducted in intact rock blocks, for example -0.57 in this study and -0.56 in Ma et al. [36]. Moreover, larger power exponents can also be found when TBM excavates in field massive rock formations, for example -0.58 and -0.55 in intact marble with thick layers [49]. Power exponents about -0.75 can only be found when the rock mass contains significant fracturing, jointing or bedding characteristics, for example -0.72 in marble with thin to medium layers [49] and -0.70, -0.79 in weathered and fractured granite [23]. Therefore, rock intactness degree can greatly affect the power exponent of the curve between rock boreability index and cutter penetration depth. For intact rock formation, this power exponent is about -0.57; for non-intact rock formation, this power exponent is about -0.75.

Rock cutting specific energy SE indicates the cutting energy input for fragmenting a unit volume of rock material. As seen in Fig. 8, when cutter penetration depth is small (e.g., 1 mm), few rock mucks are cut off, so rock cutting specific energy is quite high (about 95.9 MJ/m^3); when cutter penetration depth is high (e.g., 9 mm), rock mucks are excessively crushed into smaller chips, blocks or powders, so rock cutting specific energy is also high (about 29.8 MJ/m^3). Only when cutter penetration depth well matches the cutter spacing (i.e., p around 6 mm), large amount of elongated thick big rock mucks are produced, and rock cutting specific energy can remain low (about 10–20 MJ/m^3). This minimum point of the SE $\sim$ p curve indicates the optimum rock cutting condition and the
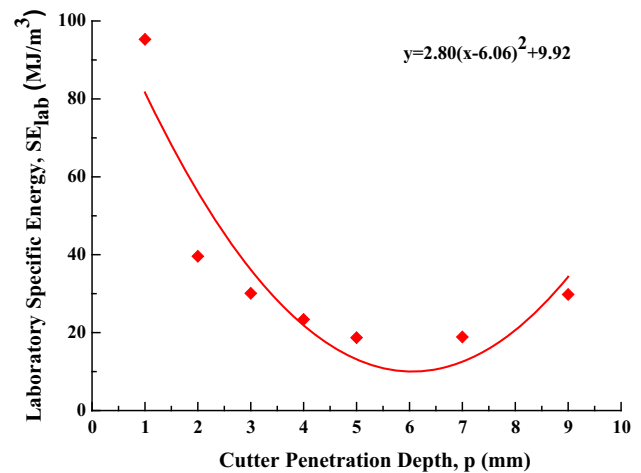
highest energy utilization condition of the disc cutting process, i.e., to use the largest portion of cutting energy input for efficient rock cutting/chipping instead of useless rock crushing/grinding. As seen in Fig. 8, for Chongqing Sandstone under cutter spacing 80 mm, the optimum cutter penetration depth is about 6.1 mm and the optimum (minimum) rock cutting specific energy is about 9.92 MJ/m^3.

3 TBM cutterhead design and the comparison with manufactured machine parameters

3.1 Input parameters for TBM cutterhead design in Chongqing Yangtze River Tunnel

Input parameters for TBM cutterhead design mainly include the predetermined parameters and laboratory-determined parameters (Table 4). From the project files, some basic project information can be pre-interpreted, for example the tunnel diameter, cutter type, etc. In Chongqing Yangtze River Tunnel, cutterhead diameter D_{TBM} is 6570 mm and 17 in. CCS (constant cross section) disc cutters are used. For most commercial 432-mm CCS disc cutters, their allowable (nominal) normal force FN_{allow} is about 250 kN and their allowable (nominal) rotational speed V_{allow} is 120 m/min. Thus, during the rock cutting process, the mean disc cutter normal force should not exceed 250 kN, and it would be better for the peak disc cutter normal force not exceeding 250 kN too much at a long period, too. The rotational speed of the outer disc cutter on the cutterhead edge should not exceed 120 m/min, which directly determines the upper limit of cutterhead rotational speed. From practical experiences, some

Table 4 Input parameters for TBM cutterhead design in Chongqing Yangtze River Tunnel

Predetermined parameters	Cutterhead diameter, D_{TBM} (mm)	6570
	Number of gauge cutters, N_G	3
	Disc cutter diameter, D (mm)	432
	Allowable disc cutter normal force, FN_{allow} (kN/cutter)	250
	Allowable cutter rotational speed, V_{allow} (m/min)	120
	Coefficient for frictional loss, f_L	1.20
	Energy transfer efficiency, k	0.85 (0.80 ∼ 0.90)
Lab-determined parameters	Cutter spacing, s (mm)	80
	Laboratory optimum cutter penetration depth, $(p_{opt})_{lab}$ (mm)	6.1
	Laboratory disc cutter normal force, $(FN_{opt})_{lab}$ (kN)	93.37
	Laboratory disc cutter rolling force, $(FR_{opt})_{lab}$ (kN)	11.74
	Laboratory specific rock mass boreability index, $SRMBI_{lab}$ (kN/mm)	44.66
	Laboratory optimum rock cutting specific energy, $(SE_{opt})_{lab}$ (MJ/m^3)	9.92

common engineering measures and adjustment factors are pre-known. For example, number of the gauge cutter N_G is usually assumed as 3, coefficient for frictional loss between cutterhead and the excavated rock mass f_L is usually assumed as 1.20 and energy transfer efficiency from the cutterhead to the tunnel face k is usually assumed between 0.80 and 0.90, averaging at 0.85 [2, 5, 13].

Laboratory-determined parameters are obtained using the above laboratory full-scale linear cutting test results, and they represent the optimum condition for rock cutting by TBM disc cutter. Practical range of the average cutter spacing s varies from 60 to 100 mm for hard rock TBMs [2, 13, 17, 20], and it is set to 80 mm in this study, just as in previous studies [35, 36]. Along with this cutter spacing 80 mm, cutter penetration depth 6.1 mm, marked as the laboratory optimum cutter penetration depth $(p_{opt})_{lab}$, corresponds to the optimum rock cutting condition. By using the curve fitting lines in Figs. 3, 4 and 8, rock cutting force and efficiency at the optimum rock cutting condition are calculated, i.e., laboratory disc cutter normal force $(FN_{opt})_{lab}$ 93.37 kN, laboratory disc cutter rolling force $(FR_{opt})_{lab}$ 11.74 kN and laboratory optimum rock cutting specific energy $(SE_{opt})_{lab}$ 9.92 MJ/m^3. From Fig. 7, laboratory specific rock mass boreability index $SRMBI_{lab}$ (BI at $p = 1.0$ mm) is calculated as 44.66 kN/mm and laboratory rock boreability index at $(p_{opt})_{lab} = 6.1$ mm is calculated as 15.93 kN/mm. It means that, in the laboratory, when disc cutter works at the optimum condition (i.e., $(p_{opt})_{lab} = 6.1$ mm), the increment of disc cutter normal force per cutter penetration depth is about 15.93 kN/mm.

3.2 Calculation procedure for TBM cutterhead design in Chongqing Yangtze River Tunnel

TBM cutterhead design, i.e., to determine the number of disc cutters, cutterhead rotational speed, thrust, torque and power, has been carried out previously by Balci [2], Bilgin et al. [5] and Copur et al. [13]. The calculation procedure is as follows:

3.2.1 Determination of number of disc cutters and cutterhead rotational speed

Number of disc cutters N_C for given cutter spacing s can be calculated using Eq. (1):

$$N_C = \frac{D_{TBM}}{2s} + N_G \tag{1}$$

Maximum cutterhead rotational speed RPM can be calculated by considering the allowable rotational speed V_{allow} for the outer disc cutter on the cutterhead edge using Eq. (2):

$$RPM = \frac{V_{allow}}{\pi D_{TBM}} \tag{2}$$

Using Eqs. (1), (2) and Table 4, the number of disc cutters N_C is calculated as 44 and maximum cutterhead rotational speed RPM is calculated as 5.8 rpm. Noting here that only the number of disc cutters (i.e., 44 single CCS disc cutter blades) can be calculated using the "open mode TBM" assumption, other detailed information about the cutting tools (e.g., multi-blade disc cutters and soft ground cutting tools) cannot be determined. Also, TBM cutterhead cannot rotate with the maximum cutterhead rotational speed 5.8 rpm, so one lower value 5.0 rpm with 15% reduction may be more acceptable.

3.2.2 Determination of cutterhead thrust and torque

Cutterhead thrust T_h and torque T_q can be calculated using Eqs. (3), (4). The input parameters are laboratory disc cutter normal and rolling forces $(FN_{opt})_{lab}$ and $(FR_{opt})_{lab}$ at optimum cutter penetration depth $(p_{opt})_{lab}$.

$$T_{\mathrm{h}} = f_{\mathrm{L}} \cdot N_{\mathrm{C}} \cdot \left(\mathrm{FN}_{\mathrm{opt}}\right)_{\mathrm{lab}} \tag{3}$$

$$T_{\mathrm{q}} = f_{\mathrm{L}} \cdot N_{\mathrm{C}} \cdot \left(\mathrm{FR}_{\mathrm{opt}}\right)_{\mathrm{lab}} \cdot 0.25 D_{\mathrm{TBM}} \tag{4}$$

Using Eqs. (3), (4) and Table 4, cutterhead thrust T_{h} is calculated as 4930 kN and cutterhead torque T_{q} is calculated as 1018 kN m. Considering that ratios of the peak to mean values of the disc cutter normal and rolling forces are both around 2.0 [2, 9, 20] and the conservative design to avoid the peak cutterhead thrust and torque exceeding the machine capacity, the designed cutterhead thrust and torque are doubled, being 9860 kN and 2036 kN m, respectively.

3.2.3 Determination of cutterhead power and instantaneous cutting rate

Cutterhead power P can be calculated by considering the cutterhead torque T_{q} and cutterhead rotational speed RPM using Eq. (5):

$$P = 2\pi \frac{\mathrm{RPM}}{60} T_{\mathrm{q}} \tag{5}$$

Production rate, i.e., instantaneous cutting rate ICR, can be calculated using Eq. (6). The input parameters are cutterhead power P and optimum (minimum) rock cutting specific energy $(\mathrm{SE}_{\mathrm{opt}})_{\mathrm{lab}}$, or optimum cutter penetration depth $(p_{\mathrm{opt}})_{\mathrm{lab}}$, cutterhead rotational speed RPM and tunnel face area A.

$$\mathrm{ICR} = k \frac{P}{\left(\mathrm{SE}_{\mathrm{opt}}\right)_{\mathrm{lab}}} \tag{6.1}$$

(based on optimum rock cutting specific energy)

$$\mathrm{ICR} = \left(p_{\mathrm{opt}}\right)_{\mathrm{lab}} \cdot \mathrm{RPM} \cdot A \tag{6.2}$$

(based on optimum cutter penetration depth)

Using Eq. (5) and Table 4, cutterhead power P is calculated as 533 kW. Considering 20% conservative design, by multiplying coefficient 1.2, the designed cutterhead power P is 640 kW. Using Eqs. (6.1) or (6.2) and Table 4, the instantaneous cutting rate ICR is calculated as 45.7 or 62.0 m³/h.

3.3 Comparison of the designed and manufactured machine parameters

Table 5 compares the designed machine parameters based on laboratory full-scale linear cutting test results and the manufactured machine parameters for the TBM used in Chongqing Yangtze River Tunnel. Detailed information about this project can be found in Sect. 4. As seen in Table 5, the designed and manufactured machine parameters are highly and well correlated; some of them are even very close, for example the average cutter spacing s (80 and 82.5 mm), the maximum cutterhead rotational speed RPM (both about 5.0 rpm) and the cutterhead power P (640 and 630 kW). However, as seen in Table 5, some of them are not so close, for example the number and type of cutters, cutterhead thrust T_{h} and torque T_{q}. This difference can be generally attributed to the different machine types. From laboratory full-scale linear cutting test results, open-mode TBM with very small opening ratio is designed, but in the field, slurry pressure balance (SPB) TBM with high opening ratio 28% is used. The setting of eight rock mucking buckets and several soft ground cutting tools (76 drag bits and eight scrapers) makes the proper layout of 44 single disc cutters very difficult. To ensure the cutterhead stiffness and as a consequence to the increased cutterhead opening ratio, a smaller number of disc cutter blades (39 instead of 44) and multi-blade disc cutters (four triple, nine double and nine single) are used. This partly leads to the difference of cutterhead thrust and torque between the designed and manufactured values. Generally, laboratory full-scale linear cutting test results, combined with some engineering considerations, can be well used for the preliminary and rough design of TBM machine capacity.

Table 5 Comparison of the designed and manufactured machine parameters

Machine parameters	Designed value	Manufactured value
Machine type	Open-mode TBM	Slurry pressure balance (SPB) TBM by Herrenknecht
Number of cutters, N_{C}	44 single CCS disc cutters	39 CCS disc cutter blades (four triple, nine double and nine single); 76 drag bits; eight scrapers
Cutter spacing, s	80 mm	82.5 mm (average value for disc cutter blades)
Cutterhead rotational speed, RPM	Up to 5.8 (or 5.0) rpm	Basic values 2.0 and 4.0 rpm, varying from 0 to 5.0 rpm
Cutterhead thrust, T_{h}	9860 kN	Maximum to 37,000 kN using 14 sets of thrust cylinders
Cutterhead torque, T_{q}	2036 kN·m	Breakout torque 3500 kN m; nominal torque 3050 kN m at 2.0 rpm and 1450 kN m at 4.0 rpm
Cutterhead power, P	640 kW	Driving power 630 kW
Instantaneous cutting rate, ICR	45.7 or 62.0 m³/h	

4 Field TBM excavation performance and the comparison with laboratory test results

4.1 Description of Chongqing Yangtze River Tunnel [45]

As seen in Fig. 9, Chongqing Yangtze River Tunnel is constructed for transporting the wastewater collected from the right side of Jialing River and the left side of Yangtze River to the south side of Yangtze River. In the tunnel cross section, three prestressed concrete cylinder pipes (PCCPs) with inner diameter 2000 mm for wastewater disposal and one steel pipe with inner diameter 600 mm for water transport are placed. This tunnel passes through the Yangtze Riverbed with minimum overburden 20 m and excavation length 925 m. As seen in Fig. 9, rock formations along the tunnel axis are mainly comprised of mudstone, sandstone and siltstone with monocline and interbedded outcrops, and their proportions in the total tunnel length are 61.40, 30.50 and 8.10%, respectively. Most of the transition sections between these mudstone formations and sandstone formations show gradually changing features with no obvious interface boundaries, and only in few locations can these sudden changes in ground conditions be easily observed. Along the tunnel axis, uniaxial compressive strength of the mudstone changes from 7.3 to 21.9 MPa and uniaxial compressive strength of the sandstone changes from 26.7 to 69.4 MPa. The sandstone samples used for standard mechanical property testing and full-scale linear cutting test are obtained from the same rock formation where TBM tunnels through, and they generally represent the upper strength limit of the sandstone formation (UCS being 60.76 MPa as in Table 1). Permeability of the mudstone formations changes from 0.02 to 0.10 md, and they can well restrain the permeation process of groundwater in the water-rich formations. Permeability of the sandstone formations changes from 0.10 to 0.30 md, up to 3.65 md; therefore, high groundwater permeation and flow can be expected in these formations. The seepage pressure of groundwater depends on the water level of Yangtze River and the buried depth of the aquifers, and 0.64 MPa is used in the machine design and excavation operation. In order to cope with the high risk of groundwater ingress and tunnel face instability during TBM tunneling, slurry pressure balance (SPB) TBM is selected. When tunneling through sandstone formations, TBM operates with open mode, only disc cutters work to fragment the rock mass; when tunneling through mudstone formations, TBM operates with SPB mode that can balance the ground and water pressure on the tunnel face.

During the construction stage, TBM tunnels through the soft mudstone formations, medium hard sandstone formations and mixed-face ground conditions (Fig. 9). In the
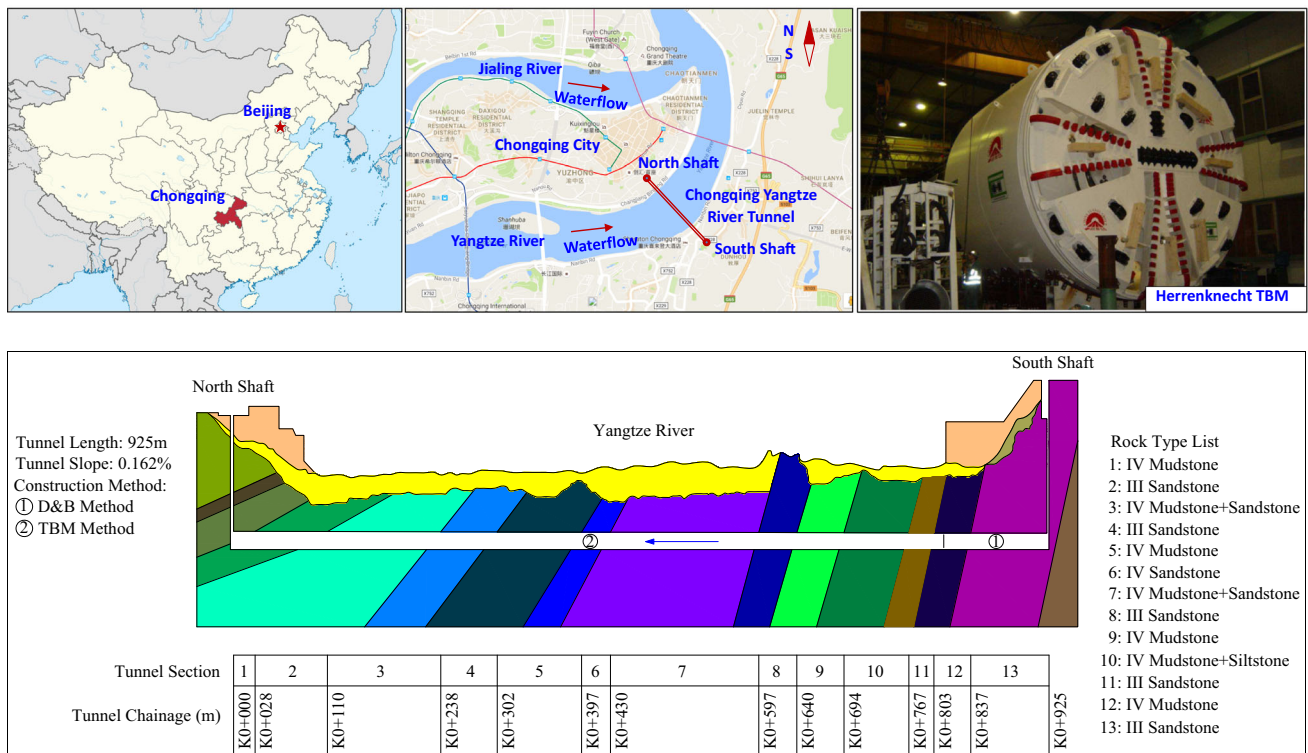

Fig. 9 Location map of Chongqing Yangtze River Tunnel and its geological cross section

clayey mudstone formations, the muddy paste formed by the loosened material and groundwater remained between the tunnel face and cutterhead may deteriorate the mechanical performance of the cutterhead from stable and effective rotation into unstable and ineffective rotation. The soft mudstone material may be not capable of generating sufficient rolling force for disc cutters to overcome the pre-torque of the cutter bearing and may block the space between cutter saddle and cutterhead plate. Both of these two situations can cause the sudden stoppage of cutter rotation and further the severe flat wear of the cutter rings. In the abrasive sandstone formations with high quartz content (about 30%), high normal cutter wear and abnormal cutter wear (e.g., flat and multi-flat wear) are also expected. Therefore, both hard rock disc cutters (four triple-, nine double- and nine single-blade ones) and soft rock cutting tools (76 drag bits and eight scrapers) and large cutterhead opening ratio (28%) are selected.

4.2 Field TBM excavation performance in Chongqing Yangtze River Tunnel

Field TBM excavation performance data are recorded when TBM tunnels through the sandstone formations using open mode, as shown in Table 6. Field disc cutter normal and rolling forces FN_{field} and FR_{field} are extracted after considering the friction loss between cutterhead and the surrounding rock mass using Eqs. (3), (4) back forward. Noting here that 39 disc cutter blades are used in the field, N_C is equal to 39 here. After determining FN_{field} and FR_{field}, field disc cutter cutting coefficient CC_{field}, normalized resultant force NRF_{field} and rock boreability index BI_{field} are calculated according to Sect. 2.1.3. Field rock cutting specific energy SE_{field} is calculated using cutterhead torque T_q, penetration depth per revolution p_{rev} and tunnel face area A. Results of the field TBM excavation performance can also be found in Song [45].

As seen in Table 6, penetration depth per revolution p_{rev} mainly changes from 2.4 to 14.5 mm, though a few unusual high values up to 23.1 mm can be observed in the field. Frenzel et al. [14] denoted that, for low-strength rocks (mostly UCS below 50 MPa), the TBM operation mode is penetration limited and the penetration depth per revolution should not exceed 15.0 mm for a long period, consistent with the field results of this study. As seen in Table 6, field cutterhead thrust T_h mainly changes from 3830.0 to 6670.0 kN, and its upper value is quite lower than the designed value 9860 kN and the manufactured value 37,000 kN. It is partly due to that the excavated rock formations have low compressive strength (only up to 69.4 MPa) and so machine thrust capability has some extent of reserve. As seen in Table 6, field cutterhead torque T_q mainly changes from 408.8 to 2098.3 kN m, and

its upper value is nearly equal to the designed value 2036 kN m and a little lower than the nominal value 3050 kN m at 2.0 rpm. It indicates that the machine torque capability is well and nearly fully utilized and thus TBM operates at torque-limited mode in excavating the sandstone formations (UCS from 26.7 to 69.4 MPa), consistent with Frenzel et al. [14]. As seen in Table 6, upper bounds of the mean values of the field disc cutter normal and rolling forces (i.e., 142.52 and 27.30 kN) are within the capacity of 17 in. CCS disc cutter (e.g., 250 kN for normal force), but the peak value of the field disc cutter normal force (i.e., 285.04 kN) has already exceeded 250 kN. As seen in Table 6, field disc cutter cutting coefficient CC_{lab} mainly changes from 6.31 to 20.59%, which means that the disc cutter rolling force can be as high as one-fifth of the disc cutter normal force. As seen in Table 6, field rock cutting specific energy SE_{field} mainly changes from 28.91 to 117.87 MJ/m^3, and thus the maximum value is four times higher than the minimum value. It means that the cutting energy input for excavating the sandstone formations is sensitive to TBM operation from 2.4 to 14.5 mm/rev.

Field TBM excavation operation is mainly done by controlling the cutterhead thrust and torque. As seen from Data Nos. 23 and 24 in Table 6, nearly equal cutterhead thrusts (i.e., 5840.0 and 5870.0 kN) are selected; however, strengths of the encountered rock mass are different. In Data No. 23, low-strength rock mass (perhaps due to the existence of fractures and joints) leads to high penetration depth per revolution (i.e., 11.2 mm); in Data No. 24, high-strength rock mass (perhaps due to the existence of higher strength rock dykes) leads to low penetration depth per revolution (i.e., 4.3 mm). The former one is normal and effective rock disc cutting, disc cutter resultant force acts on the middle point of the rock-cutter contact arc and bisects the rock-cutter contact angle to pass through the cutter hub (NRF_{field} being 0.5018) and rock boreability index is quite lower (BI_{field} being 11.14 kN/mm). The latter one is abnormal and ineffective rock disc cutting, disc cutter resultant force acts more transversally to the disc cutter and may bend the cutter saddle by high impact/shock (NRF_{field} being 0.8974) and rock boreability index is relatively higher (BI_{field} being 29.17 kN/mm).

4.3 Comparison of the laboratory full-scale linear cutting test results with field TBM excavation performance data

4.3.1 Laboratory and field disc cutter normal and rolling forces

As seen in Fig. 10, at same cutter penetration depth, field disc cutter normal force is higher than laboratory disc

Table 6 Field TBM excavation performance data in open mode for Chongqing Yangtze River Tunnel

No.	T_h (kN)	T_q (kN·m)	p_{rev} (mm)	FN_{field} (kN)	FR_{field} (kN)	CC_{field} (%)	NRF_{field} (Ratio)	BI_{field} (kN/mm)	SE_{field} (MJ/m³)
1	3830.0	425.7	2.4	81.84	5.54	6.77	0.4528	34.10	111.75
2	3930.0	408.8	2.4	83.97	5.32	6.33	0.4239	34.99	116.36
3	4060.0	507.5	2.6	86.75	6.60	7.61	0.4891	33.37	105.09
4	4149.1	763.1	3.7	88.66	9.93	11.20	0.6016	23.96	99.21
5	4169.6	773.5	3.8	89.09	10.06	11.29	0.5987	23.45	88.22
6	4214.5	796.2	4.1	90.05	10.36	11.50	0.5868	21.96	97.13
7	4250.0	736.0	3.0	90.81	9.57	10.54	0.6295	30.27	98.08
8	4298.5	840.0	4.3	91.85	10.93	11.90	0.5925	21.36	88.40
9	4535.8	971.9	5.0	96.92	12.64	13.05	0.6017	19.38	73.48
10	4578.0	996.6	4.8	97.82	12.96	13.25	0.6239	20.38	84.75
11	4855.9	1169.3	5.3	103.76	15.21	14.66	0.6558	19.58	40.80
12	4880.0	505.7	2.6	104.27	6.58	6.31	0.4057	40.11	117.87
13	5005.5	1269.7	6.5	106.96	16.52	15.44	0.6230	16.45	37.52
14	5043.1	1295.8	5.5	107.76	16.86	15.64	0.6862	19.59	42.41
15	5049.4	1300.1	6.7	107.89	16.91	15.68	0.6227	16.10	34.17
16	5083.6	1324.2	3.5	108.62	17.23	15.86	0.8725	31.04	96.22
17	5407.3	1565.6	6.0	115.54	20.37	17.63	0.7386	19.26	38.27
18	5410.0	1416.0	6.9	115.60	18.42	15.94	0.6235	16.75	35.93
19	5449.8	1836.0	9.2	116.45	23.88	20.51	0.6907	12.66	33.74
20	5506.6	918.0	3.8	117.66	11.94	10.15	0.5385	30.96	92.25
21	5585.2	1709.3	6.0	119.34	22.24	18.63	0.7797	19.89	35.94
22	5591.9	1714.8	6.5	119.49	22.31	18.67	0.7505	18.38	35.95
23	5840.0	1570.6	11.2	124.79	20.43	16.37	0.5018	11.14	28.91
24	5870.0	1748.2	4.3	125.43	22.74	18.13	0.8974	29.17	93.44
25	5894.6	1978.5	9.2	125.95	25.74	20.44	0.6882	13.69	35.91
26	5910.0	1831.0	8.0	126.28	23.82	18.86	0.6829	15.79	35.89
27	5920.8	2002.5	10.3	126.51	26.05	20.59	0.6550	12.28	32.45
28	6210.0	1847.0	10.1	132.69	24.03	18.11	0.5835	13.14	29.14
29	6210.0	1725.3	8.9	132.69	22.44	16.91	0.5817	14.91	30.35
30	6270.0	1869.0	11.3	133.97	24.31	18.15	0.5526	11.86	32.45
31	6390.0	1936.0	12.0	136.54	25.19	18.45	0.5447	11.38	32.15
32	6440.0	1777.7	10.7	137.61	23.13	16.81	0.5268	12.86	31.64
33	6530.0	2075.1	14.5	139.53	27.00	19.35	0.5186	9.62	40.16
34	6670.0	2098.3	14.4	142.52	27.30	19.15	0.5153	9.90	48.18
Min.	3830.0	408.8	2.4	81.84	5.32	6.31	0.4057	9.62	28.91
Max.	6670.0	2098.3	14.5	142.52	27.30	20.59	0.8974	40.11	117.87

T_h cutterhead thrust, T_q cutterhead torque, p_{rev} penetration depth per revolution, FN_{field} field disc cutter normal force, FR_{field} field disc cutter rolling force, CC_{field} field disc cutter cutting coefficient, NRF_{field} field disc cutter normalized resultant force, BI_{field} field rock boreability index, SE_{field} field rock cutting specific energy

cutter normal force, and the increasing rate of the former curve is higher than that of the latter curve, too. Like laboratory FN ~ p curve in Sect. 2.2.1, there also exists exponential function relation between field disc cutter normal force FN_{field} and penetration depth per revolution p_{rev}. Moreover, penetration depth per revolution 5.0 mm and field disc cutter normal force 106.10 kN seem to mark one critical threshold, below which field disc cutter normal force per penetration depth per revolution is larger than

5 kN and above which field disc cutter normal force per penetration depth per revolution is smaller than 5 kN. This critical threshold (5.0 mm and 106.10 kN) denoting field rock disc cutting process from difficulty to ease is in good agreement with the laboratory test results in Sect. 2.2.1. However, the field values are much higher than the laboratory values (i.e., 3.0 mm and 76.56 kN). As seen in Table 7, field disc cutter normal force is generally more than 1.20 times higher than laboratory disc cutter normal
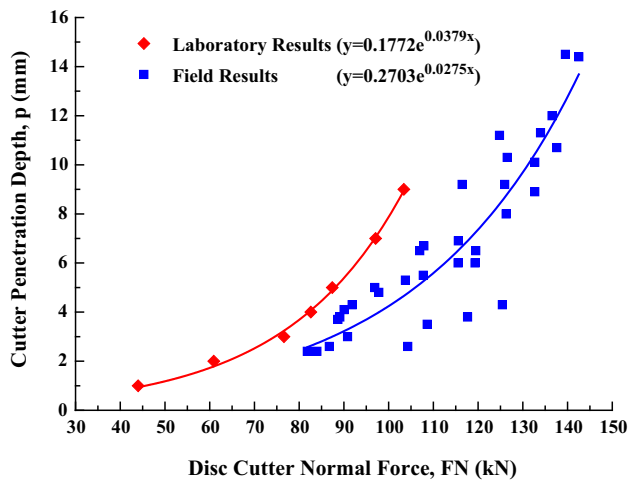
Fig. 10 Comparison between laboratory and field disc cutter normal forces (FN_{lab} and FN_{field})

force at same cutter penetration depth, especially for cutter penetration depth above 5.0 mm. Moreover, at the optimum rock cutting conditions, field disc cutter normal force is about 1.42 times higher than laboratory disc cutter normal force (i.e., $FN_{field} = 132.28$ kN at $p_{rev} = 10.3$ mm and $FN_{lab} = 93.37$ kN at $p = 6.1$ mm).

As seen in Fig. 11, at same cutter penetration depth, field disc cutter rolling force is higher than laboratory disc

cutter rolling force, and the increasing rate of the former curve is higher than that of the latter curve, too. Like laboratory FR $\sim p$ curve in Sect. 2.2.1, there also exists linear function relation between field disc cutter rolling force FR_{field} and penetration depth per revolution p_{rev}. Also, no critical threshold can be marked for FR_{field} $\sim p$ curve, consistent with the laboratory test results in Sect. 2.2.1. As seen in Fig. 11, when disc cutter penetrates 1 mm deeper, increment about 2.3 kN is required for field disc cutter rolling force, slightly higher than the laboratory test results (about 1.8 kN). As seen in Table 7, field disc cutter rolling force is generally more than 1.30 times higher than laboratory disc cutter rolling force at the same cutter penetration depth. Moreover, at the optimum rock cutting conditions, field disc cutter rolling force is about 2.19 times higher than laboratory disc cutter rolling force (i.e., $FR_{field} = 25.68$ kN at $p_{rev} = 10.3$ mm and $FR_{lab} = 11.74$ kN at $p = 6.1$ mm).

4.3.2 Laboratory and field disc cutter cutting coefficient and normalized resultant force

As seen in Fig. 12, at the same cutter penetration depth, field disc cutter cutting coefficient is higher than laboratory disc cutter cutting coefficient, but the increasing rate of the former curve is lower than that of the latter curve. It means

Table 7 Comparison of the laboratory full-scale linear cutting test results and field TBM excavation performance data

p (mm)	Disc cutter normal force (kN)			Disc cutter rolling force (kN)			Boreability index (kN/mm)			Specific energy (MJ/m^3)		
	FN_{lab}	FN_{field}	$\frac{FN_{field}}{FN_{lab}}$	FR_{lab}	FR_{field}	$\frac{FR_{field}}{FR_{lab}}$	BI_{lab}	BI_{field}	$\frac{BI_{field}}{BI_{lab}}$	SE_{lab}	SE_{field}	$\frac{SE_{field}}{SE_{lab}}$
1	45.66	47.57	1.04	2.50	4.22	1.69	44.66	69.53	1.56	81.61	152.86	1.87
2	63.95	72.78	1.14	4.31	6.53	1.51	30.08	41.92	1.39	56.07	126.87	2.26
3	74.65	87.52	1.17	6.12	8.83	1.44	23.88	31.18	1.31	36.14	103.84	2.87
4	82.24	97.98	1.19	7.94	11.14	1.40	20.26	25.27	1.25	21.80	83.77	3.84
5	88.12	106.10	1.20	9.75	13.45	1.38	17.84	21.47	1.20	13.07	66.66	5.10
6	92.93	112.73	1.21	11.56	15.76	1.36	16.08	18.80	1.17	9.93	52.51	5.29
7	97.00	118.33	1.22	13.38	18.06	1.35	14.73	16.80	1.14	12.39	41.32	3.33
8	100.53	123.19	1.23	15.19	20.37	1.34	13.65	15.24	1.12	20.46	33.09	1.62
9	103.63	127.47	1.23	17.00	22.68	1.33	12.76	13.98	1.10	34.12	27.82	0.82
10	106.41	131.30	1.23	18.81	24.99	1.33	12.02	12.95	1.08	53.39	25.52	0.48
11	108.93	134.77	1.24	20.63	27.29	1.32	11.38	12.08	1.06	78.25	26.17	0.33
12	111.22	137.93	1.24	22.44	29.60	1.32	10.83	11.33	1.05	108.71	29.78	0.27
13	113.34	140.84	1.24	24.25	31.91	1.32	10.35	10.69	1.03	144.78	36.35	0.25
14	115.29	143.54	1.25	26.07	34.22	1.31	9.92	10.13	1.02	186.44	45.88	0.25
15	117.11	146.05	1.25	27.88	36.52	1.31	9.54	9.63	1.01	233.71	58.37	0.25
Opt.[a]	93.37	132.38	1.42	11.74	25.68	2.19	15.93	12.67	0.80	9.92	25.40	2.56

All the values are obtained from the curve fitting lines, not real laboratory or field results. In this case, it is assumed that the two curve fitting lines using laboratory and field results are valid in the cutter penetration depth ranging from 1 to 15 mm

[a]Opt. means the optimum value of the corresponding parameter. The optimum values for laboratory full-scale linear cutting test are obtained at cutter penetration depth $p = 6.1$ mm, and the optimum values for field TBM excavation performance are obtained at penetration depth per revolution $p_{rev} = 10.3$ mm
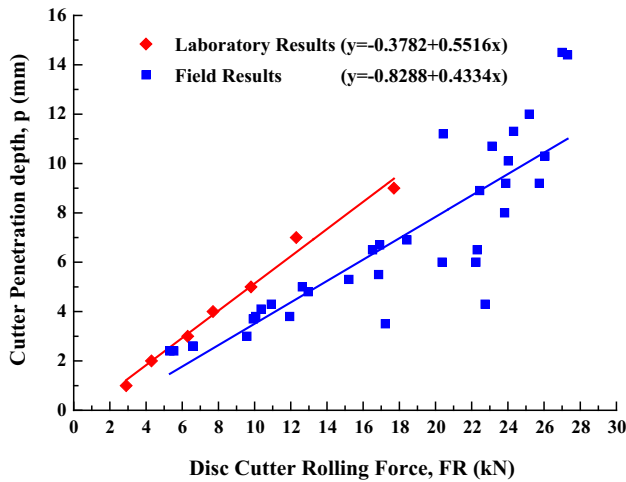
Fig. 11 Comparison between laboratory and field disc cutter rolling forces (FR_{lab} and FR_{field})
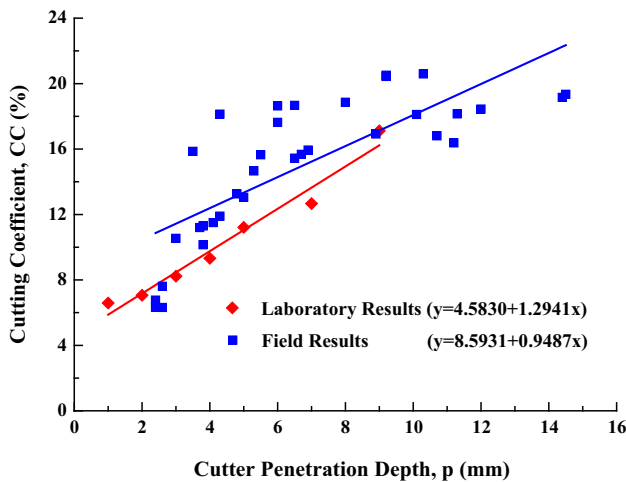

Fig. 12 Comparison between laboratory and field cutting coefficients (CC_{lab} and CC_{field})

that the field and laboratory disc cutter cutting coefficients differ greatly at low cutter penetration depth and then they become closer at high cutter penetration depth. Like laboratory $CC \sim p$ curve in Sect. 2.2.2, there also exists linear function relation between field disc cutter cutting coefficient CC_{field} and penetration depth per revolution p_{rev}, though this trend is not so obvious. As seen in Fig. 12, when disc cutter penetrates 1 mm deeper, increment about 1.0% is required for field disc cutter cutting coefficient, slightly lower than the laboratory test results (about 1.2%).

As seen in Fig. 13, field disc cutter normalized resultant forces are generally larger than laboratory disc cutter normalized resultant forces since their average values are 0.6128 and 0.5389, respectively. It means that, in the field, disc cutter resultant force acts higher above the midpoint of
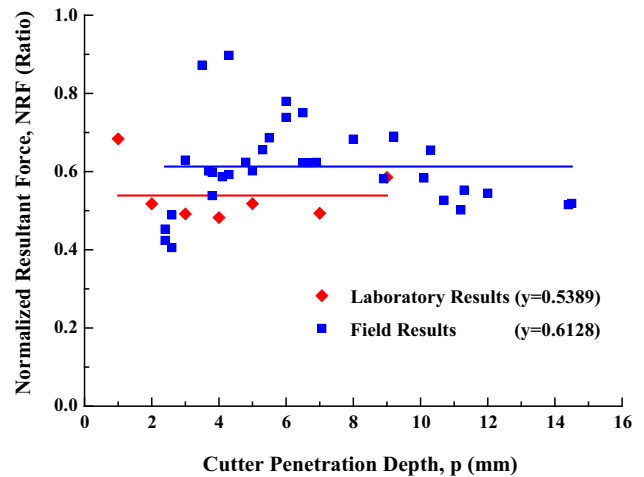

Fig. 13 Comparison between laboratory and field normalized resultant forces (NRF_{lab} and NRF_{field})

the rock-cutter contact arc and also acts higher above the force acting point in the laboratory. In the field, disc cutter normalized resultant forces are more scattered distributed than those in the laboratory, minimum to 0.4057 and maximum to 0.8974. It indicates the more irregular and challenging rock cutting condition in the field, i.e., the highly varying acting point and acting direction of the disc cutter resultant force.

4.3.3 Laboratory and field rock boreability index and rock cutting specific energy

As seen in Fig. 14, at same cutter penetration depth, field rock boreability index is higher than laboratory rock boreability index. Like laboratory BI $\sim p$ curve in Sect. 2.2.3, there also exists power function relation between field rock boreability index BI_{field} and penetration
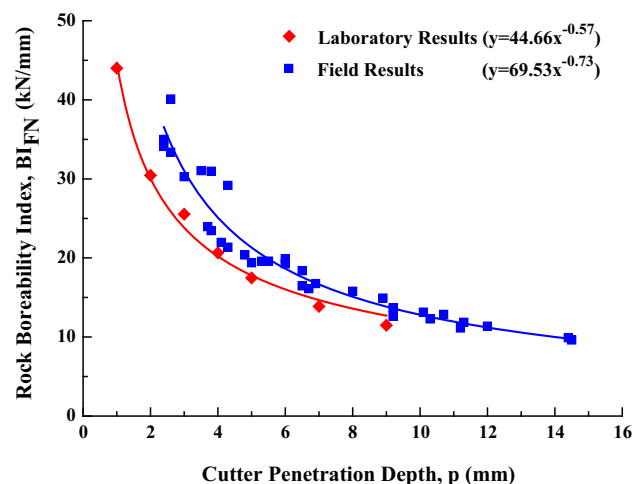

Fig. 14 Comparison between laboratory and field rock boreability indices (BI_{lab} and BI_{field})

depth per revolution p_{rev}. Moreover, penetration depth per revolution 8.0 mm seems to mark one critical threshold, below which field rock boreability index is high and decreases rapidly and above which field rock boreability index is low and decreases slowly. This result is consistent with the laboratory test results in Sect. 2.2.3, though the field value is much higher than the laboratory value (i.e., 5.0 mm). Field specific rock mass boreability index ($SRMBI_{field}$) is calculated as 69.53 kN/mm, higher at some extent than the laboratory one ($SRMBI_{lab}$) 44.66 kN/mm. The phenomenon that $SRMBI_{field}$ is larger than $SRMBI_{lab}$ can also be found in Balci [2] where $SRMBI_{field}$ is 172.89 kN/mm and $SRMBI_{lab}$ are 78.43 and 27.05 kN/mm, and Copur et al. [13] where $SRMBI_{field}$ are 12.7 and 18.9 kN/mm and $SRMBI_{lab}$ are 10.47 and 8.72 kN/mm. This can be partly attributed to the lack of confining stress in laboratory rock cutting tests and the existence of in situ stress in field TBM excavation process. The involvement of confining stressed condition will restrain rock cutting by TBM disc cutter and thus increases the rock boreability index BI, as demonstrated by Ma et al. [36]. Moreover, the power exponent of field BI $\sim p$ curve is -0.73, quite close to the suggested one -0.75 [23, 49] and much smaller than the laboratory one -0.57. This result again proves the conclusion in Sect. 2.2.3: For fractured/jointed rock mass, the power exponent of the BI $\sim p$ curve is more close to -0.75; for intact/massive rock mass, the power exponent of the BI $\sim p$ curve is much larger than -0.75, being about -0.57. As seen in Fig. 14, the two curves, i.e., $BI_{field} \sim p$ and $BI_{lab} \sim p$ curves, become more close and then overlap at high cutter penetration depth. As seen in Table 7, at the optimum rock cutting conditions, field rock boreability index is about 0.80 times smaller than laboratory rock boreability index (i.e., $BI_{field} = 12.67$ kN/mm at $p_{rev} = 10.3$ mm and $BI_{lab} = 15.93$ kN/mm at $p = 6.1$ mm).

As seen in Fig. 15, there exist both quadratic function relations between field and laboratory rock cutting specific energies and cutter penetration depth, i.e., $SE_{field} \sim p$ and $SE_{lab} \sim p$ curves, and the $SE_{field} \sim p$ curve generally is located above the $SE_{lab} \sim p$ curve. That is to say, in the field, we can also find one minimum value of rock cutting specific energy, which is higher than the minimum value in the laboratory, to determine the optimum rock cutting condition. The minimum value phenomenon in this study is not marked in Balci [2] where field rock cutting specific energy keeps decreasing when penetration depth per revolution increases till to 16 mm/rev. This difference can be partly due to the rock intactness degree: The rock formations in Kozyatagi-Kadikoy Metro Tunnel are highly fractured [2] while the rock formations in Chongqing Yangtze River Tunnel are somewhat massive and less fractured. As stated by Balci [2], fractured characteristics
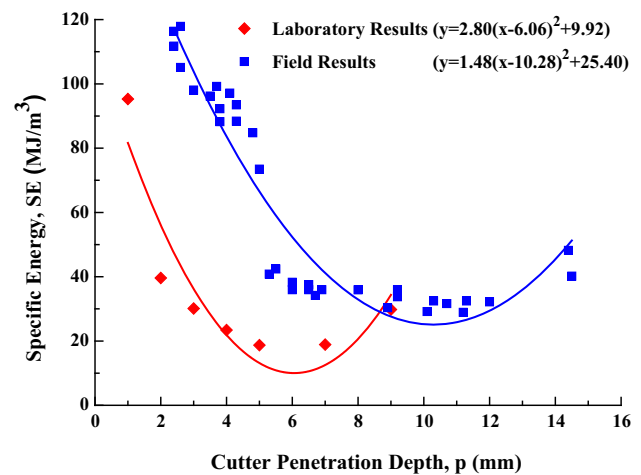

Fig. 15 Comparison between laboratory and field rock cutting specific energies (SE_{lab} and SE_{field})

of the rock formation can affect tremendously TBM performance and thus the predicted values based on laboratory test results may differ from the field data at a large extent due to the highly fractured characteristic of the rock formation excavated. As seen in Fig. 15, laboratory optimum cutter penetration depth $(p_{opt})_{lab}$ is about 6.1 mm while field optimum cutter penetration depth $(p_{opt})_{field}$ is much larger, being about 10.3 mm. The phenomenon that $(p_{opt})_{lab}$ is smaller than $(p_{opt})_{field}$ can also be found in Balci [2] where $(p_{opt})_{lab}$ is 8.0 mm and $(p_{opt})_{field}$ is 16.0 mm, and Copur et al. [13] where $(p_{opt})_{lab}$ are 7.0 and 11.0 mm and $(p_{opt})_{field}$ are 9.7 and 13.0 mm. As seen in Fig. 15, laboratory optimum rock cutting specific energy $(SE_{opt})_{lab}$ is about 9.92 MJ/m^3 while field optimum rock cutting specific energy $(SE_{opt})_{field}$ is quite larger, being about 25.40 MJ/m^3. The phenomenon that $(SE_{opt})_{lab}$ is smaller than $(SE_{opt})_{field}$ can also be found in Balci [2] where $(SE_{opt})_{lab}$ are 4.1 and 3.0 kW h/m^3 mm and $(SE_{opt})_{field}$ is 7.7 kW h/m^3, and Copur et al. [13] where $(SE_{opt})_{lab}$ are 4.33 and 3.65 kW h/m^3 and $(SE_{opt})_{field}$ are 8.4 and 5.9 kW h/m^3. The two results clearly indicate that TBM has to penetrate much deeper in the field than in the laboratory to obtain the optimum rock cutting condition and meanwhile much higher rock cutting specific energy is required in the field than in the laboratory.

4.4 Correlation of the laboratory full-scale linear cutting test results with field TBM excavation performance data

Laboratory full-scale linear cutting tests are conducted in intact large rock blocks without confining stress by using one disc cutter at penetration-controlled mode, but field TBM tunneling is operated in fractured/jointed rock mass with overburden and in situ stress using the whole

cutterhead at thrust/torque-controlled mode. Rock intactness degree, confining stressed condition and rock cutting mode can surely affect the results both in the laboratory and in the field. As seen in Figs. 10, 11, 12, 13 and 15, the changing trends of these rock cutting results with increasing cutter penetration depth in the field, i.e., exponential function type of FN, linear function type of FR, CC and NRF, power function type of BI and quadratic function type of SE, can be well predicted using the laboratory test results, but their magnitudes in the field are generally much higher than those in the laboratory. As seen in Tables 7 and 8, for the optimum rock cutting condition in Chongqing Sandstone and Chongqing Yangtze River

Tunnel, the field to laboratory ratios of these rock cutting results are much higher than 1.00, even with unacceptable difference. For cutter penetration depth, this ratio is 1.69; for disc cutter normal force, this ratio is 1.42; for disc cutter rolling force, this ratio is 2.19; for rock boreability index, this ratio is 0.80; and for rock cutting specific energy, this ratio is 2.56. As seen in Table 5, the manufactured machine parameters can be well predicted using the laboratory test results, some of them are very close (e.g., s, RPM and P) and some of them are not so close for design compromises (e.g., N_C, T_h and T_q). Therefore, TBM cutterhead design based on laboratory full-scale linear cutting tests is accurate, reliable and applicable at some

Table 8 Correlation of the laboratory full-scale linear cutting test results and field TBM excavation performance data

Target variable	Laboratory value	Field value	Ratio value	Modification factor	Project name
Cutter penetration depth (mm)	$(p_{opt})_{lab}$	$(p_{opt})_{field}$	$(p_{opt})_{field}/(p_{opt})_{lab}$	K_p	
	6.1	10.3	1.69	1.51	Chongqing Yangtze River Tunnel
	8.0	16.0[a]	2.00		Kozyatagi-Kadikoy Metro Tunnel
	7.0	9.7[a]	1.39		Kartal-Kadikoy Metro Tunnel
	11.0	13.0[a]	1.18		Otogar-Bagcilar Metro Tunnel (1)
	10.0	13.0[a]	1.30		Otogar-Bagcilar Metro Tunnel (2)
Disc cutter normal force (kN)	$(FN_{opt})_{lab}$	$(FN_{opt})_{field}$	$(FN_{opt})_{field}/(FN_{opt})_{lab}$	K_{FN}	
	93.37	132.38	1.42	1.78	Chongqing Yangtze River Tunnel
	81.9	135.0	1.65		Kozyatagi-Kadikoy Metro Tunnel
	73.32	102.13	1.39		Kartal-Kadikoy Metro Tunnel
	95.9	192.5	2.01		Otogar-Bagcilar Metro Tunnel (1)
	95.5	231.0	2.42		Otogar-Bagcilar Metro Tunnel (2)
Disc cutter rolling force (kN)	$(FR_{opt})_{lab}$	$(FR_{opt})_{field}$	$(FR_{opt})_{field}/(FR_{opt})_{lab}$	K_{FR}	
	11.74	25.68	2.19	2.32	Chongqing Yangtze River Tunnel
	8.6	29.5	3.43		Kozyatagi-Kadikoy Metro Tunnel
	9.1	21.64	2.38		Kartal-Kadikoy Metro Tunnel
	12.0	13.37	1.11		Otogar-Bagcilar Metro Tunnel (1)
	12.1	30.0	2.48		Otogar-Bagcilar Metro Tunnel (2)
Rock boreability index (kN/mm)	$(BI_{opt})_{lab}$	$(BI_{opt})_{field}$	$(BI_{opt})_{field}/(BI_{opt})_{lab}$	K_{BI}	
	15.93	12.67	0.80	1.37	Chongqing Yangtze River Tunnel
	10.24	8.44	0.82		Kozyatagi-Kadikoy Metro Tunnel
	10.47	12.7	1.21		Kartal-Kadikoy Metro Tunnel
	8.72	18.9	2.17		Otogar-Bagcilar Metro Tunnel (1)
	9.55	17.77	1.86		Otogar-Bagcilar Metro Tunnel (2)
Rock cutting specific energy (MJ/m³)	$(SE_{opt})_{lab}$	$(SE_{opt})_{field}$	$(SE_{opt})_{field}/(SE_{opt})_{lab}$	K_{SE}	
	9.92	25.40	2.56	1.90	Chongqing Yangtze River Tunnel
	12.96[b]	23.04[b]	1.78		Kozyatagi-Kadikoy Metro Tunnel
	15.59[b]	30.24[b]	1.94		Kartal-Kadikoy Metro Tunnel
	13.14[b]	21.24[b]	1.62		Otogar-Bagcilar Metro Tunnel (1)
	13.32[b]	21.24[b]	1.59		Otogar-Bagcilar Metro Tunnel (2)

Chongqing Yangtze River Tunnel is from this study, Kozyatagi-Kadikoy Metro Tunnel is from Balci [2], Kartal-Kadikoy Metro Tunnel and Otogar-Bagcilar Metro Tunnel (1) are from Copur et al. [13], Otogar-Bagcilar Metro Tunnel (2) is from Balci and Tumac [3]

If not available in the original reference papers, these values will be calculated from cutterhead thrust and torque by using Eqs. (3), (4) and the calculation method in Sect. 2.1.3

[a] In fact, these values are the average penetration depths per revolution of the cutterhead in the field. No optimum cutter penetration depth can be marked in the field for these tunnel projects due to the highly fractured nature of the excavated rock formations

[b] In the original reference papers [2, 3, 13], these optimum rock cutting specific energy values are not expressed in international system of units (SI) and thus their unit is transferred from kW h/m³ into MJ/m³ in this study

extent (Table 5). However, TBM performance prediction based on laboratory full-scale linear cutting tests can differ greatly from those in the field, and thus modification factors are required (Table 7).

Along with Chongqing Yangtze River Tunnel, comparisons between the laboratory and field results at the optimum rock cutting conditions from other four tunnel projects are also summarized in Table 8. As seen, most of these ratios, 23 in 25, are much higher than 1.00, maximum to 3.43; few of these ratios, 2 in 25, are slightly lower than 1.00, being about 0.80. The very high optimum cutter penetration depth in the field (16.0 mm) over the one in the laboratory (8.0 mm) for Kozyatagi-Kadikoy Metro Tunnel is explained by Balci [2] as attributed to fractured nature of the rock mass which is having average 21% RQD. The very high disc cutter normal and rolling forces in the field (135.0 and 29.5 kN) over the ones in the laboratory (81.9 and 8.6 kN) for Kozyatagi-Kadikoy Metro Tunnel are explained by Balci [2] as mainly due to the high frictional forces between shield and highly fractured or almost loose blocky rock formation in front of the TBM, and this also causes an increase in power, torque and specific energy requirements. The very high optimum rock cutting specific energy in the field (23.04 MJ/m^3) over the one in the laboratory (12.96 MJ/m^3) for Kozyatagi-Kadikoy Metro Tunnel is explained by Balci [2] as mainly caused by the inefficient cutting process of the TBM where big-sized muck blocks are circulated in front of the TBM to be crushed into small pieces to pass within the openings of the cutterhead and sometimes the fine material in front of the TBM increases frictional forces with torque and specific energy. From Copur et al. [13], it can be summarized that, for Kartal-Kadikoy Metro Tunnel, laboratory full-scale linear cutting test works well at some extent for predicting optimum cutter penetration depth (7.0 and 9.7 mm), disc cutter normal force (73.32 and 102.13 kN) and rock boreability index (10.47 and 12.7 kN/mm), but it does not predict accurately disc cutter rolling force (9.1 and 21.64 kN) and optimum rock cutting specific energy (13.14 and 21.24 MJ/m^3) due to the frictional resistance of the loose rock in the half-filled cutterhead chamber. From Copur et al. [13], it can be summarized that, for Otogar-Bagcilar Metro Tunnel (1), laboratory full-scale linear cutting test works well at some extent for predicting optimum cutter penetration depth (11.0 and 13.0 mm) and disc cutter rolling force (12.0 and 13.37 kN), but it does not predict accurately disc cutter normal force (95.9 and 192.5 kN) and rock boreability index (8.72 and 18.9 kN/mm) due to the V-type disc cutter blunting and the friction between the TBM shield and the ground.

Therefore, the influence factors that make the predicted TBM excavation performance from laboratory test results differ from the field data can be divided into three categories, i.e., the fractured/jointed/bedded and squeezing/frictional characteristics of the excavated rock formation, the overburden and in situ stress condition along the tunnel axis and the rock excavation mode. The last one includes the number and type of the cutting tools (CCS- or V-type and single- or multi-blade disc cutter, hard rock or soft ground cutting tools), layout of the cutterhead (opening ratio, cutter arrangement, etc.) and TBM operation mode (open mode, half-closed mode or closed mode). These influence factors can cause very wide ranges of the field to laboratory ratios (Table 8), for example for disc cutter rolling force ranging from 1.11 to 3.43. However, by averaging the field to laboratory ratios from these five tunnel projects, it is still possible to obtain five modification factors to predict TBM excavation performance more close to field data based on the laboratory test results, as follows:

$$\left(p_{\text{opt}}\right)_{\text{field}} = 1.51\left(p_{\text{opt}}\right)_{\text{lab}} \tag{7}$$

$$\left(\text{FN}_{\text{opt}}\right)_{\text{field}} = 1.78\left(\text{FN}_{\text{opt}}\right)_{\text{lab}} \tag{8}$$

$$\left(\text{FR}_{\text{opt}}\right)_{\text{field}} = 2.32\left(\text{FR}_{\text{opt}}\right)_{\text{lab}} \tag{9}$$

$$\left(\text{BI}_{\text{opt}}\right)_{\text{field}} = 1.37\left(\text{BI}_{\text{opt}}\right)_{\text{lab}} \tag{10}$$

$$\left(\text{SE}_{\text{opt}}\right)_{\text{field}} = 1.90\left(\text{SE}_{\text{opt}}\right)_{\text{lab}} \tag{11}$$

The parameters in the left part of these five equations correspond to the optimum rock cutting condition in field TBM excavation processes, and the parameters in the right part of these five equations correspond to the optimum rock cutting condition in laboratory rock cutting tests. Although these modification factors are scattered distributed for specific tunnel projects (e.g., averaging at 2.32 and ranging from 1.11 to 3.43 for disc cutter rolling force of these five tunnel projects), the employment of these modification factors can surely reduce the difference between the laboratory test results and field TBM excavation performance data, at least to some extent. For example, after using the modification factors for Chongqing Sandstone, the predicted and field results are: for optimum cutter penetration depth 9.2 and 10.3 mm, for disc cutter normal force 176.47 and 132.38 kN, for disc cutter rolling force 27.24 and 25.68 kN, for rock boreability index 21.82 and 12.67 kN/mm and for optimum rock cutting specific energy 18.85 and 25.40 MJ/m^3. As seen, the prediction results after modification can predict the optimum cutter penetration depth and disc cutter rolling force at high accuracy and optimum rock cutting specific energy at some extent. However, the prediction results after modification still cannot well predict the disc cutter normal force and rock boreability index, which needs further investigations.

5 Conclusions

In this study, determination of some machine parameters and performance prediction for tunnel boring machine (TBM) are conducted based on the laboratory full-scale linear cutting test results; the predicted and field results are compared to investigate the similarities and differences between laboratory rock cutting test and field TBM excavation performance. The main works and conclusions can be drawn as follows:

(1) The changing trends of disc cutter normal and rolling forces, cutting coefficient, force acting point, rock boreability index and rock cutting specific energy with increasing cutter penetration depth are deeply analyzed. Results show that, for Chongqing Sandstone, cutter penetration depth 3.0 mm denotes the start of efficient rock cutting by TBM disc cutter and cutter penetration depth 5.0 mm denotes the mechanical rock breakage from difficulty to ease. Meanwhile, cutter penetration depth 6.1 mm denotes the optimum rock cutting condition and the optimum (minimum) rock cutting specific energy is about 9.92 MJ/m^3.

(2) Input parameters for TBM cutterhead design are extracted; some TBM specifications are determined and then compared to the manufactured values. Results show that, for Chongqing Sandstone, the designed and manufactured machine parameters are highly and well correlated, some of them are very close, for example average cutter spacing, cutterhead rotational speed and cutterhead power, but some of them are not so close for design compromises, for example number of cutters, cutterhead thrust and torque.

(3) Laboratory full-scale linear cutting test results in Chongqing Sandstone are compared with the field TBM excavation performance data in Chongqing Yangtze River Tunnel. Results show that the changing trends of the rock cutting results with increasing cutter penetration depth in the field can be well predicted using the laboratory test results, i.e., the exponential function type of disc cutter normal force, the linear function type of disc cutter rolling force, cutting coefficient and force acting point, the power function type of rock boreability index and the quadratic function type of rock cutting specific energy. However, their magnitudes in the field are generally much higher than the values in the laboratory.

(4) Generally, the predicted TBM excavation performance based on the laboratory test results can differ from the field performance data due to the discontinuity characteristic of the rock formation, the in situ stress condition along the tunnel alignment and the rock excavation mode. However, by employing some modification factors (much larger than 1.00), the differences between laboratory rock cutting tests and field TBM excavation performance can be surely reduced, at least to some extent. More field and laboratory tests under different rock cutting conditions are still needed to generalize and improve the modification method proposed in this study.

References

1. Abu Bakar MZ, Gertsch L, Rostami J (2014) Evaluation of fragments from disc cutting of dry and saturated sandstone. Rock Mech Rock Eng 47(5):1891–1903. https://doi.org/10.1007/s00603-013-0482-8

2. Balci C (2009) Correlation of rock cutting tests with field performance of a TBM in a highly fractured rock formation: a case study in Kozyatagi-Kadikoy metro tunnel, Turkey. Tunn Undergr Space Technol 24(4):423–435. https://doi.org/10.1016/j.tust.2008.12.001

3. Balci C, Tumac D (2012) Investigation into the effects of different rocks on rock cuttability by a V-type disc cutter. Tunn Undergr Space Technol 30(4):183–193. https://doi.org/10.1016/j.tust.2012.02.018

4. Barton N (2000) TBM tunnelling in jointed and faulted rock. Balkema, Rotterdam

5. Bilgin N, Copur H, Balci C, Tumac D, Akgul M, Yuksel A (2008) The selection of a TBM using full scale laboratory tests and comparison of measured and predicted performance values in Istanbul Kozyatagi-Kadikoy metro tunnels. In: World tunnel congress 2008-underground facilities for better environment and safety, India

6. Bruland A (1998) Hard rock tunnel boring. Ph.D. thesis, Norwegian University of Science and Technology, Trondheim, Norway

7. Cardu M, Iabichino G, Oreste P, Rispoli A (2017) Experimental and analytical studies of the parameters influencing the action of TBM disc tools in tunnelling. Acta Geotech 12(2):293–304. https://doi.org/10.1007/s11440-016-0453-9

8. Chen LH, Labuz JF (2006) Indentation of rock by wedge-shaped tools. Int J Rock Mech Min Sci 43(7):1023–1033. https://doi.org/10.1016/j.ijrmms.2006.03.005

9. Cho JW, Jeon S, Yu SH, Chang SH (2010) Optimum spacing of TBM disc cutters: a numerical simulation using the three-dimensional dynamic fracturing method. Tunn Undergr Space Technol 25(3):230–244. https://doi.org/10.1016/j.tust.2009.11.007

10. Cho JW, Jeon S, Jeong HY, Chang SH (2013) Evaluation of cutting efficiency during TBM disc cutter excavation within a Korean granitic rock using linear-cutting-machine testing and

photogrammetric measurement. Tunn Undergr Space Technol 35(4):37–54. https://doi.org/10.1016/j.tust.2012.08.006

11. Choi SW, Chang SH, Park YT, Lee GP, Bae GJ (2014) Comparative analysis of cutter acting forces and axial stresses of single and double disc cutters by linear cutting tests. J Korean Tunn Undergr Space Assoc 16(2):181–191. https://doi.org/10.9711/KTAJ.2014.16.2.181 (in Korean)

12. Commission on Engineering and Technical Systems of USA (1984) Geotechnical site investigation for underground projects 2:182. http://www.nap.edu/html/919/NI000102.pdf. Accessed 1 Aug 2017

13. Copur H, Aydin H, Bilgin N, Balci C, Tumac D, Dayanc C (2014) Predicting performance of EPB TBMs by using a stochastic model implemented into a deterministic model. Tunn Undergr Space Technol 42(3):1–14. https://doi.org/10.1016/j.tust.2014.01.006

14. Frenzel C, Käsling H, Thuro K (2008) Factors influencing disc cutter wear. Geomech Tunn 1:55–60. https://doi.org/10.1002/geot.200800006

15. Fukui K, Okubo S (1999) Rock-properties estimation by TBM cutting force. In: 9th international congress on rock mechanics, vol 2, pp 1217–1220

16. Fukui K, Okubo S (2006) Some attempts for estimating rock strength and rock mass classification from cutting force and investigation of optimum operation of tunnel boring machines. Rock Mech Rock Eng 39(1):25–44. https://doi.org/10.1007/s00603-005-0071-6

17. Geng Q, Wei ZY, Meng H, Chen Q (2016) Numerical and experimental research on the rock-breaking process of tunnel boring machine normal disc cutters. J Mech Sci Technol 30(4):1733–1745. https://doi.org/10.1007/s12206-016-0329-9

18. Gertsch R (1993) Tunnel boring machine disk cutter vibrations. MS thesis, Colorado School of Mines, Golden, USA

19. Gertsch R (2000) Rock toughness and disc cutting. Ph.D. thesis, University of Missouri, Rolla, USA

20. Gertsch R, Gertsch L, Rostami J (2007) Disc cutting tests in Colorado Red Granite: implications for TBM performance prediction. Int J Rock Mech Min Sci 44(2):238–246. https://doi.org/10.1016/j.ijrmms.2006.07.007

21. Gong QM, Zhao J, Jiao YY (2005) Numerical modeling of the effects of joint orientation on rock fragmentation by TBM cutters. Tunn Undergr Space Technol 20:183–191. https://doi.org/10.1016/j.tust.2004.08.006

22. Gong QM, Jiao YY, Zhao J (2006) Numerical modelling of the effects of joint spacing on rock fragmentation by TBM cutters. Tunn Undergr Space Technol 21:46–55. https://doi.org/10.1016/j.tust.2005.06.004

23. Gong QM, Zhao J, Jiang YS (2007) In situ TBM penetration tests and rock mass boreability analysis in hard rock tunnels. Tunn Undergr Space Technol 22(3):303–316. https://doi.org/10.1016/j.tust.2006.07.003

24. Gong QM, Zhao J (2009) Development of a rock mass characteristics model for TBM penetration rate prediction. Int J Rock Mech Min Sci 46(1):8–18. https://doi.org/10.1016/j.ijrmms.2008.03.003

25. Gong QM, He GW, Zhao XB, Ma HS, Li XZ, Zhang H, Miao CT (2015) Influence of different cutter spacings on rock fragmentation efficiency of Beishan granite by TBM. Chin J Geotech Eng 37(1):54–60 (in Chinese)

26. Gong QM, Dong GL, Yin LJ, Ma S, Lu JW (2016) Comparison study on the rock linear and rotating cutting tests by TBM cutter. Constr Technol 46(11):61–66 (in Chinese)

27. Gong QM, Du XL, Li Z, Wang QX (2016) Development of a mechanical rock breakage experimental platform. Tunn Undergr Space Technol 57:129–136. https://doi.org/10.1016/j.tust.2016.02.019

28. Gong QM, He GW, Zhao XB, Zhang H, Miao CT, Yao XH, Li XZ (2016) Influence of penetration on the rock-breakage efficiency of a TBM cutter. Mod Tunn Technol 53(1):62–68. https://doi.org/10.13807/j.cnki.mtt.2016.01.010 (in Chinese)

29. Gong QM, Yin LJ, Ma HS, Zhao J (2016) TBM tunnelling under adverse geological conditions: an overview. Tunn Undergr Space Technol 57:4–17. https://doi.org/10.1016/j.tust.2016.04.002

30. Liu QS, Liu JP, Pan YC, Kong XX, Cui XZ, Huang SB, Wei L (2016) Research advances of tunnel boring machine performance prediction models for hard rock. Chin J Rock Mech Eng 35(S1):2766–2786. https://doi.org/10.13722/j.cnki.jrme.2014.1601 (in Chinese)

31. Liu QS, Pan YC, Liu JP, Kong XX, Shi K (2016) Comparison and discussion on fragmentation behavior of soft rock in multi-indentation tests by a single TBM disc cutter. Tunn Undergr Space Technol 57:151–161. https://doi.org/10.1016/j.tust.2016.02.021

32. Liu QS, Pan YC, Kong XX, Liu JP, Shi K, Cui XZ, Huang SB (2016) Experimental investigation on mudstone fragmentation characteristics in indentation process by TBM disc cutter. Rock Soil Mech 37(S1):166–174. https://doi.org/10.16285/j.rsm.2016.S1.022 (in Chinese)

33. Liu QS, Pan YC, Liu JP, Kong XX, Shi K, Liu Q (2016) Analysis on fragmentation behavior of rocks in indentation tests by disc cutter. Chin J Rock Mech Eng 35(S2):3516–3525. https://doi.org/10.13722/j.cnki.jrme.2015.0532 (in Chinese)

34. Ma HS, Yin LJ, Ji HG (2011) Numerical study of the effect of confining stress on rock fragmentation by TBM cutters. Int J Rock Mech Min Sci 48(6):1021–1033. https://doi.org/10.1016/j.ijrmms.2011.05.002

35. Ma HS, Gong QM, Wang J, Yin LJ, Zhao XB (2016) Study on the influence of confining stress on TBM performance in granite rock by linear cutting test. Tunn Undergr Space Technol 57:145–150. https://doi.org/10.1016/j.tust.2016.02.020

36. Ma HS, Gong QM, Wang J, Zhao XB, Yin LJ, Miao CT, He GW (2016) Linear cutting tests on effect of confining stress on rock fragmentation by TBM cutter. Chin J Rock Mech Eng 35(2):346–355. https://doi.org/10.13722/j.cnki.jrme.2014.0926 (in Chinese)

37. Moon T, Oh J (2012) A study of optimal rock-cutting conditions for hard rock TBM using the discrete element method. Rock Mech Rock Eng 45(5):837–849. https://doi.org/10.1007/s00603-011-0180-3

38. Ramezanzadeh A, Rostami J, Kastner R (2003) Performance prediction models for hard rock tunnel boring machines. http://iransaze.com/files-for-download/maghale/mohandesi%20tonel/konferans-mohandesi-tonel/Performance%20Prediction%20Models%20for%20Hard%20Rock%20Tunnel%20Boring%20Machines.pdf. Accessed 1 Aug 2017

39. Rostami J (1991) Design optimization, performance predictions, and economic analysis of TBM application in the proposed Yucca mountain nuclear waste repository. MS thesis 4139, Colorado School of Mines, Golden, USA

40. Rostami J, Ozdemir L (1993) A new model for performance prediction of hard rock TBMs. In: Proceedings of rapid excavation and tunneling conference. USA, pp 794–809. http://emi.mines.edu/UserFiles/File/earthMechanics/disc_cutters/disc_cutter1.PDF. Accessed 1 Aug 2017

41. Rostami J, Ozdemir L, Nilson B (1996) Comparison between CSM and NTH hard rock TBM performance prediction models. http://emi.mines.edu/UserFiles/File/earthMechanics/seminar/08_01_machine_performance_assessment_and_costing.pdf?textonly=1. Accessed 1 Aug 2017

42. Rostami J (2013) Study of pressure distribution within the crushed zone in the contact area between rock and disc cutters. Int J

Rock Mech Min Sci 57(1):172–186. https://doi.org/10.1016/j.ijrmms.2012.07.031

43. Roxborough FF, Phillips HR (1975) Rock excavation by disc cutter. Int J Rock Mech Min Sci Geomech Abstr 12(75):361–366. https://doi.org/10.1016/0148-9062(75)90547-1

44. Sanio HP (1985) Prediction of the performance of disc cutters in anisotropic rock. Int J Rock Mech Min Sci Geomech Abstr 22(3):153–161. https://doi.org/10.1016/0148-9062(85)93229-2

45. Song KZ (2005) Analysis on shield driving performance of a tunnel under river in alternation of mud rock and sand rock bed. Ph.D. thesis. Beijing Jiaotong University, Beijing, China (**in Chinese**)

46. Tumac D, Balci C (2015) Investigations into the cutting characteristics of CCS type disc cutters and the comparison between experimental, theoretical and empirical force estimations. Tunn Undergr Space Technol 45:84–98. https://doi.org/10.1016/j.tust.2014.09.009

47. Tuncdemir H, Bilgin N, Copur H, Balci C (2008) Control of rock cutting efficiency by muck size. Int J Rock Mech Min Sci 45(2):278–288. https://doi.org/10.1016/j.ijrmms.2007.04.010

48. Ulusay R, Hudson JA (2007) The complete ISRM suggested methods for rock characterization, testing and monitoring: 1974–2006. International Society for Rock Mechanics, Ankara

49. Yin LJ, Gong QM, Zhao J (2014) Study on rock mass boreability by TBM penetration test under different in situ stress conditions. Tunn Undergr Space Technol 43(7):413–425. https://doi.org/10.1016/j.tust.2014.06.002

50. Yin LJ, Miao CT, He GW, Dai FC, Gong QM (2016) Study on the influence of joint spacing on rock fragmentation under TBM cutter by linear cutting test. Tunn Undergr Space Technol 57:137–144. https://doi.org/10.1016/j.tust.2016.02.018